

## Research Article

# Analysis of Complex Modal Characteristics of Fractional Derivative Viscoelastic Rotating Beams

Tianle Lu, Zhongmin Wang , and Dongdong Liu

*School of Civil Engineering and Architecture, Xi'an University of Technology, 710048 Xi'an, China*

Correspondence should be addressed to Zhongmin Wang; wangzhongm@xaut.edu.cn

Received 28 May 2019; Revised 21 July 2019; Accepted 17 September 2019; Published 16 October 2019

Guest Editor: Franco Concli

Copyright © 2019 Tianle Lu et al. This is an open access article distributed under the Creative Commons Attribution License, which permits unrestricted use, distribution, and reproduction in any medium, provided the original work is properly cited.

For the transverse vibration problem of a fractional derivative viscoelastic rotating beam, the differential equation of the system is obtained based on the Euler–Bernoulli beam theory and Hamilton principle. Then, introducing dimensionless quantities to differential equations and boundary conditions, the generalized complex eigenvalue equations of the system are obtained by the differential quadrature method. The effects of the slenderness ratio, the viscoelastic ratio, the hub radius–beam length ratio, and dimensionless hub speed and fractional order on the vibration characteristics of fractional derivative viscoelastic rotating beams are discussed by numerical examples. Numerical calculations show that when the dimensionless hub speed is constant, the real part of complex frequency increases with the increase of the fractional order, and the higher-order growth trend is more obvious. Through the study of displacement response at different points on the beam, it can be seen that the closer to the free end, the larger the response amplitude. And, the amplitude of response has been attenuated, which is also consistent with the vibration law of free vibration considering damping.

## 1. Introduction

With the rapid development of manufacturing industry and mechanical structure engineering, rotating structure is more and more widely used in mechanical engineering, such as internal combustion engines, satellites, turbines, and CNC machine tools.

Many scholars have made a lot of research on the dynamics of rotating beams. Bannerjee and Su [1] analyzed the free vibration characteristics of Timoshenko beams by the dynamic stiffness method and compared the results with Euler–Bernoulli theory. In consideration of Coriolis force and centrifugal force, Tian et al. [2] investigated the influence of hub radius, slenderness ratio, and angular velocity on the vibration characteristics of rotating beam. Aksencer and Aydogdu [3] studied the vibration problem of rotating composite beams by using the Ritz method, and the effects of several geometric factors on the vibration characteristics of composite beams under different boundary conditions were analyzed. Considering geometric nonlinearity, Zhang et al. [4] studied the nonlinear vibration of a variable cross-section

viscoelastic rotating beam, which is based on Kelvin–Voigt viscoelastic constitutive relation, and the amplitude–frequency response of the rotating beam is obtained by the multiscale method. Li et al. [5] studied the vibration characteristics of a rotating FGM circular section flexible beam. Srivatsa and Ranjan [6] solved the vibration problem of a rotating Rayleigh beam with variable cross-section and obtained the frequency and mode shapes of the beam by the finite element method. Tang et al. [7] investigated the free vibration of the rotating cone cantilever beam based on the Hamiltonian principle, and then analyzed the effects of angular velocity and the moment of inertia on the free vibration of the system. Sofiyev and Hui [8] used FOSDT and Donnell shell theory to study the vibration and stability of cylindrical shells with functionally graded materials under mixed boundary conditions and analyzed the influence of factors such as FG distribution on the critical parameters of FGMCSS containing MBCS. Based on FOSDT and isotropic constitutive relation, Yao et al. [9] studied the nonlinear dynamic response of a rotating cylindrical shell with pretorsion angle by using Hamilton principle, and the effects of

excitation parameters, damping coefficient, rotational speed, prerotation angle, and pretorsion angle on the nonlinear dynamic response of the system were analyzed. Based on the dynamic stiffness method, Banerjee and Jackson [10] investigated the free vibration characteristics of the rotating cone-shaped Rayleigh beam and analyzed the effects of the viscosity-elasticity rate on the free vibration characteristics of the rotating conical Rayleigh beam. Based on Euler–Bernoulli, Timoshenko, Reid, and Levison’s four different beam theories, Chakraverty and Behera [11] used the DQM to investigate the buckling of nanobeams and analyzed the effects of nonlocal parameters, aspect ratio, boundary conditions, and nonuniform parameters on the critical buckling load parameters.

The fractional derivative viscoelastic model is considered to be a model that can accurately describe the constitutive relation of viscoelastic materials, and it can describe the mechanical behavior of materials in a wide frequency range and determine the experimental parameters required for the model. Based on fractional derivative theory, Gao et al. [12] investigated the viscoelastic mechanical parameters of three standard linear solid material properties. Tarasov [13] investigated the characteristics of fractional derivatives of noninteger order and proposed the nonlocality principle of fractional derivatives. Achouri et al. [14] investigated the initial-boundary value problem of Euler–Bernoulli beam equation with fractional derivative boundary conditions and analyzed the existence and attenuation of its initial-boundary value solution. Based on Euler–Bernoulli beam theory, Ansari et al. [15] studied the geometric nonlinearity vibration of fractional order viscoelastic nanobeams. Bahraini et al. [16] studied the free vibration of viscoelastic cantilever beams with different boundary conditions under concentrated loads and analyzed the influence of fractional derivatives on the large deflection of viscoelastic cantilever beams.

At present, the theory and application of the differential quadrature method (DQM) are quite mature, and it is mainly used to solve some problems such as high-order differential equations with variable coefficients. Li and Ying [17] solved the transverse vibration of elastic Euler–Bernoulli beams under interharmonic loads by the differential quadrature method and analyzed its vibration characteristics. Based on the Euler–Bernoulli beam model, Zhang et al. [18] studied the large deformation mechanical behavior of members by the differential quadrature method. Cao [19] investigated the static response of reinforced concrete (RC) beams using the generalized differential quadrature method by virtual work principle. Through the differential quadrature method, Matbuluy et al. [20] solved the free vibration problem of functionally graded elastic beams and studied the influence of geometric parameters on the natural frequency of the beam. Li et al. [21] studied the dynamic properties of viscoelastic Timoshenko beams by the differential quadrature method and the nonlinear numerical method. Considering the geometric parameters, moment of inertia, and quadratic coupling deformations of variable cross-section beams, Wang and Li [22] studied the transverse vibration characteristics of a rotating cone cantilever beam by using

Hamiltonian variational principle, and the DQM was used to solve the differential equation of motion. Based on the thin plate theory, Zhou and Wang [23] solved the vibration problem of variable thickness viscoelastic plates by the differential quadrature method and studied the influence of length to diameter ratio and thickness to diameter ratio on the vibration of linear thickness viscoelastic plates.

In this paper, based on Euler–Bernoulli beam theory and Hamilton principle, the vibration model and motion differential equation of the fractional derivative viscoelastic rotating beam are established. The dimensionless quantity is introduced, and the differential equations and boundary conditions are processed in a dimensionless manner. Then, the differential quadrature method is used to discretize the differential equation and boundary conditions, and the generalized complex eigenequation of the system is obtained. The effects of slenderness ratio, the hub radius-beam length ratio, the viscoelastic ratio, dimensionless hub speed, and fractional order on the complex frequency characteristics of the system are analyzed.

## 2. One-Dimensional Fractional Kelvin–Voigt Model Theory

The classical Kelvin–Voigt model is composed of a spring and a Newton viscous pot in parallel, and the stress-strain relationship of the fractional Kelvin model is as follows:

$$\sigma_x(t) = E\varepsilon_x(t) + \eta D^\alpha [\varepsilon_x(t)], \quad (1)$$

where  $E$  and  $\eta$  are the Young’s modulus of elasticity and damping modulus of the material,  $\varepsilon_x(t)$  is the Lagrange strain of finite deformation;  $D^\alpha$  is the Riemann–Liouville fractional differential operator, and  $\alpha$  is a fractional order.

Set  $0 \leq \alpha \leq 1$ , the  $\alpha$  order Riemann–Liouville fractional derivative of the function  $f(t)$  defined on  $[0, t]$  is expressed as follows [12]:

$$D^\alpha [f(t)] = \frac{f(0)}{\Gamma(1-\alpha)} t^{-\alpha} + \frac{1}{\Gamma(1-\alpha)} \int_0^t \frac{f'(\tau)}{(t-\tau)^\alpha} d\tau. \quad (2)$$

## 3. Differential Equation of Motion

**3.1. Deformation Field Description.** Figure 1(a) shows that the schematic diagram of the fractional derivative viscoelastic rotating hollow beam, which has length  $L$  of the beam, radius  $a$ , and rotating angular velocity  $\omega$  of the hub. The  $oxy$  and  $OXY$  are the floating coordinate system and the inertial coordinate system, respectively. The  $\theta$  represents rotation angle of the viscoelastic beam in a wide range of motion, that is, the rotation angle of the  $oxy$  is relative to the  $OXY$ . The  $ox$ -axis coincides with the axis of the viscoelastic hollow circular section beam before deformed.

In Figure 1(b), the cross-section of the beam is a hollow section with wall thickness  $h$  and  $R_n$  is the radius of the wall thickness for any cross-section at the middle line. In the  $n-s$  coordinate system,  $n$  is the normal direction and  $s$  is the tangential direction.

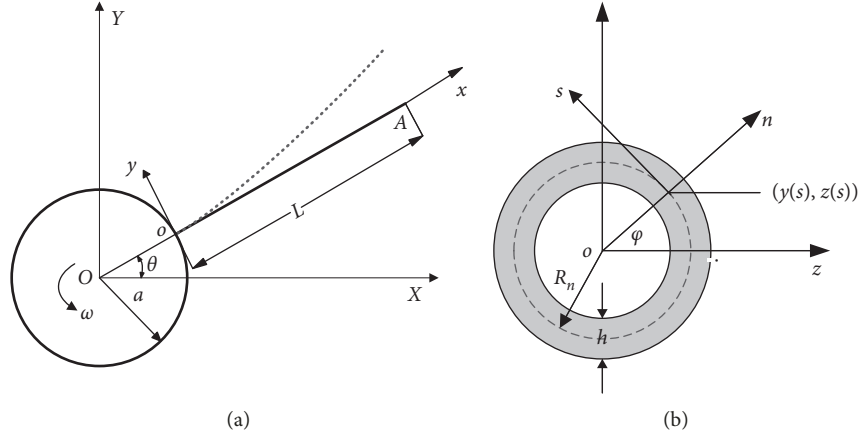


FIGURE 1: Dynamic model of fractional derivative viscoelastic rotating hollow beam. (a) Fractional derivative viscoelastic rotating hollow beam. (b) Viscoelastic rotating hollow beam profile.

In Figure 2,  $\mathbf{r}_a$  is a radius vector of the hub,  $\mathbf{x}_p$  is the vector diameter of any point  $P$  on the axis of a fractional derivative viscoelastic beam relative to the point  $o$  in the floating coordinate system when it is not deformed, and  $\mathbf{u}_p$  is a displacement vector of the point  $P$ .

The position vector of point  $P$  relative to the point  $O$  can be written as follows:

$$\mathbf{r}_p = \mathbf{r}_a + \mathbf{A}_\theta(\mathbf{x}_p + \mathbf{u}_p), \quad (3)$$

where

$$\begin{aligned} \mathbf{r}_a &= [a \cos \theta \quad a \sin \theta]^T, \\ \mathbf{x}_p &= [x \quad 0]^T, \\ \mathbf{A}_\theta &= \begin{bmatrix} \cos \theta & -\sin \theta \\ \sin \theta & \cos \theta \end{bmatrix}, \\ \mathbf{u}_p &= \begin{bmatrix} u_{px} \\ u_{py} \end{bmatrix} = \begin{bmatrix} u + u_c + u_b \\ w \end{bmatrix} \\ &= \begin{bmatrix} u - \frac{1}{2} \int_0^x (w_{,x})^2 dx - y w_{,x} \\ w \end{bmatrix}, \end{aligned} \quad (4)$$

where  $\mathbf{A}_\theta$ ,  $u$ , and  $w$  are the transformation matrices of the  $oxy$  relative to the  $OXY$ , the axial displacement, and the lateral bending deformation displacement on the beam axis, respectively;  $u_b = -y w_{,x}$  is the axial displacement caused by the rotation of the beam cross-section,  $u_c = -1/2 \int_0^x (w_{,x})^2 dx$  is the secondary deformation coupling of the

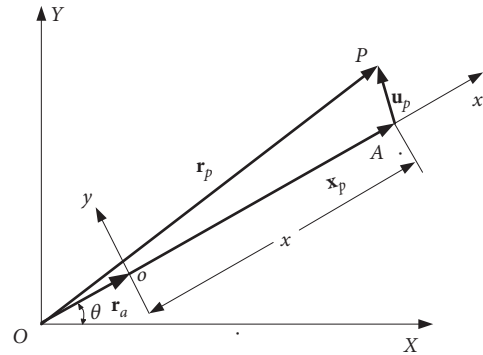


FIGURE 2: Displacement field at any point on the beam axis.

beam, that is, the axial expansion amount caused by the lateral bending deformation of the fractional derivative viscoelastic rotating hollow beam, and “ $x$ ” represents the first derivative of  $x$ .

Taking the first derivative of time for equation (3), we get the velocity vector of point  $P$  as follows:

$$\begin{aligned} \dot{\mathbf{r}}_p &= \dot{\mathbf{r}}_a + \dot{\boldsymbol{\theta}} \times \mathbf{A}_\theta(\mathbf{x}_p + \mathbf{u}_p) + \mathbf{A}_\theta \dot{\mathbf{u}}_p \\ &= \begin{bmatrix} -(a+x+u_c+u_b)\dot{\theta} \sin \theta - w\dot{\theta} \cos \theta + (\dot{u}_c + \dot{u}_b) \cos \theta - \dot{w} \sin \theta \\ (a+x+u_c+u_b)\dot{\theta} \cos \theta - w\dot{\theta} \sin \theta + (\dot{u}_c + \dot{u}_b) \sin \theta + \dot{w} \cos \theta \end{bmatrix}, \end{aligned} \quad (5)$$

where  $\dot{\boldsymbol{\theta}} = \begin{bmatrix} 0 & -\dot{\theta} \\ \dot{\theta} & 0 \end{bmatrix}$  is the antisymmetric matrix of angular velocity  $\dot{\theta}$  and “ $\dot{\cdot}$ ” represents the first derivative of  $t$ .

**3.2. Differential Equations of Motion.** The total kinetic energy of the system can be seen as the sum of the kinetic energy of the hub and the kinetic energy of the fractional derivative viscoelastic rotating beam, namely

$$\begin{aligned}
T_s &= T_H + T \\
&= \frac{1}{2}J_H\dot{\theta}^2 + \frac{1}{2}\rho \int_V \dot{\mathbf{r}}_p^T \dot{\mathbf{r}}_p dV \\
&= \frac{1}{2}J_H\dot{\theta}^2 + \frac{1}{3}\rho I \dot{\theta}^2 \int_0^L (w_{,x})^2 dx + \frac{1}{3}\rho I \int_0^L (\dot{w}_{,x})^2 dx \\
&\quad + \frac{1}{2} \int_0^L \rho A \left[ \dot{w}^2 + \dot{u}_c^2 + \dot{\theta}^2 [w^2 + (a+x+u_c)^2] \right] dx \\
&\quad + \int_0^L \rho A \dot{\theta} [-\dot{u}_c w + \dot{w}(a+x+u_c)] dx,
\end{aligned} \tag{6}$$

where  $J_H$  is the inertia moment of the hub with respect to the central axis.

The strain energy of the system can be divided into two parts, one part is potential energy and the other part is dissipative energy.

The potential energy can be expressed as follows:

$$V_0 = \int_V \frac{1}{2} \sigma_x \varepsilon_x dV = \int_V \frac{1}{2} E \varepsilon_x^2 dV, \tag{7}$$

where  $\sigma_x$ ,  $\varepsilon_x$ , and  $V$  are the normal stress, normal strains of the beam, and the volume of the viscoelastic beam, respectively.

In equation (4), not considering the axial displacement and ignoring nonlinear term, the normal strain can be obtained by the relationship between strain and displacement, namely,

$$\begin{aligned}
\varepsilon_x = u_{p,x,x} &= \left[ -\frac{1}{2} \int_0^x (w_{,x})^2 dx - y w_{,x} \right]_{,x} \\
&= -[y(s) - nz_{,s}] w_{,xx} - \frac{1}{2} (w_{,x})^2.
\end{aligned} \tag{8}$$

According to Figure 1(b), the geometric relations can be obtained:

$$\begin{aligned}
\frac{dz}{ds} &= -\sin \phi = -\sin\left(\frac{s}{R_n}\right), \\
\frac{dy}{ds} &= \cos \phi = \cos\left(\frac{s}{R_n}\right).
\end{aligned} \tag{9}$$

Then, the potential energy can be expressed as follows:

$$\begin{aligned}
V_0 &= \int_0^L \int_{A/2} \frac{1}{2} E \varepsilon_x^2(t) dA dx \\
&= \int_0^L \int_{-h/2}^{h/2} \int_0^{\pi R_n} \frac{1}{2} E \left[ (R_n + n) \sin \frac{s}{R_n} w_{,xx} + \frac{1}{2} (w_{,x})^2 \right]^2 \\
&\quad \cdot \frac{R_n + n}{R_n} ds dn dx \\
&= \frac{1}{2} EI \int_0^L (w_{,xx})^2 dx + \frac{1}{8} EA \int_0^L (w_{,x})^4 dx,
\end{aligned} \tag{10}$$

where  $I$  and  $A$  are the inertia moment and the cross-sectional area of the beam, respectively,

$$\begin{aligned}
I &= \frac{1}{64} \pi \left[ (2R_n + h)^4 - (2R_n - h)^4 \right] = \frac{1}{4} \pi (4R_n^3 h + R_n h^3), \\
A &= \pi \left[ \left( R_n + \frac{h}{2} \right)^2 - \left( R_n - \frac{h}{2} \right)^2 \right] = 2\pi R_n h.
\end{aligned} \tag{11}$$

The expression of the system's dissipative energy is

$$W_c = \int_V \int_0^{\varepsilon_x(t)} \eta D^\alpha [\varepsilon_x(t)] d\varepsilon_x(t) dV. \tag{12}$$

From equation (2), the following equation can be obtained

$$D^\alpha [\varepsilon_x(t)] = \frac{\varepsilon_x(0)}{\Gamma(1-\alpha)} t^{-\alpha} + \frac{1}{\Gamma(1-\alpha)} \int_0^t \frac{\dot{\varepsilon}_x(\tau)}{(t-\tau)^\alpha} d\tau. \tag{13}$$

Substituting equation (12) into equation (13), the following equation can be obtained:

$$\begin{aligned}
W_c &= \int_V \eta D^\alpha [\varepsilon_x(t)] \varepsilon_x(t) dV \\
&= \int_V \int_0^{\varepsilon_x(t)} \eta \frac{\varepsilon_x(0)}{\Gamma(1-\alpha)} t^{-\alpha} d\varepsilon_x(t) dV \\
&\quad + \int_V \int_0^{\varepsilon_x(t)} \eta \frac{1}{\Gamma(1-\alpha)} \int_0^t \frac{\dot{\varepsilon}_x(\tau)}{(t-\tau)^\alpha} d\tau d\varepsilon_{xx} dV \\
&= \eta I \int_0^L w_{,xx} D^\alpha (w_{,xx}) dx + \frac{1}{4} \eta A \int_0^L (w_{,x})^2 D^\alpha [(w_{,x})^2] dx.
\end{aligned} \tag{14}$$

In this paper, based on Hamiltonian variational principle, the differential equation of fractional derivative viscoelastic rotating beam is derived. Hamilton's variational principle takes the form of

$$\delta \int_{t_1}^{t_2} L dt = \delta \int_{t_1}^{t_2} (T_s - V_0 - W_c) dt = 0. \tag{15}$$

Substituting equations (6), (10), and (14) into equation (15) and ignoring the nonlinear term in the equation, the vibration differential equation of the uniformly rotating ( $\dot{\theta} = \omega_0$ ,  $\ddot{\theta} = 0$ ) fractional derivative viscoelastic beam can be obtained:

$$\begin{aligned}
&-EI w_{,xxxx} + \rho A (-\ddot{w} + \omega_0^2 w) - \frac{2}{3} \rho I \omega_0^2 w_{,xx} \\
&\quad + \frac{2}{3} \rho I \ddot{w}_{,xx} + \rho A \omega_0^2 a (L-x) w_{,xx} - \eta I D^\alpha (w_{,xxxx}) \\
&\quad + \frac{1}{2} \rho A \omega_0^2 (L^2 - x^2) w_{,xx} - \rho A \omega_0^2 (a+x) w_{,x} = 0.
\end{aligned} \tag{16}$$

The boundary conditions of the fractional derivative viscoelastic beam are as follows:

$x = 0$ :

$$w = 0, \quad (17a)$$

$$w_{,x} = 0. \quad (17b)$$

$x = L$ :

$$EIw_{,xx} + \eta ID^\alpha w_{,xx} = 0, \quad (17c)$$

$$EI \frac{\partial}{\partial x} \left( \frac{\partial^2 w}{\partial x^2} \right) - \frac{2}{3} \rho I \frac{\partial^3 w}{\partial x \partial t^2} + \frac{2}{3} \rho I \omega_0^2 \frac{\partial w}{\partial x} + \eta I \frac{\partial}{\partial x} (D^\alpha w_{,xx}) = 0. \quad (17d)$$

**3.3. Dimensional Normalization of the Equation.** To facilitate subsequent calculations, the following dimensionless quantities have been introduced:

$$\begin{aligned} \xi &= \frac{x}{L}, \\ W &= \frac{w}{L}, \\ r_0 &= \frac{a}{L}, \\ r &= \frac{R}{L}, \\ \tilde{t} &= \frac{t}{L^2 \sqrt{(\rho A/EI)}}, \\ \omega_1 &= \omega_0 L^2 \sqrt{\frac{\rho A}{EI}}, \\ g &= \frac{\eta}{EL^2 \sqrt{(\rho A/EI)}}, \end{aligned} \quad (18)$$

where  $r_0$  is the hub radius-beam length ratio,  $r$  is slenderness ratio,  $\omega_1$  is dimensionless hub speed, and  $g$  is viscoelastic ratio.

Substituting the above dimensionless quantity into equation (16)

$$\begin{aligned} \frac{\partial^4 W}{\partial \xi^4} + \frac{\partial^2 W}{\partial \tilde{t}^2} - \omega_1^2 r_0 (1 - \xi) \frac{\partial^2 W}{\partial \xi^2} + \frac{1}{6} \omega_1^2 r^2 \frac{\partial^2 W}{\partial \xi^2} \\ - \frac{1}{2} \omega_1^2 (1 - \xi^2) \frac{\partial^2 W}{\partial \xi^2} - \omega_1^2 W + g \frac{\partial^\alpha}{\partial \tilde{t}^\alpha} \left( \frac{\partial^4 W}{\partial \xi^4} \right) \\ - \frac{1}{6} r^2 \frac{\partial^4 W}{\partial \xi^2 \partial \tilde{t}^2} + \omega_1^2 (r_0 + \xi) \frac{\partial W}{\partial \xi} = 0. \end{aligned} \quad (19)$$

The solution of equation (19) can be set as  $W(\xi, \tilde{t}) = W(\xi) \exp(\omega_f \tilde{t})$ , and the differential equation of mode shape can be written as follows:

$$\begin{aligned} W_{,\xi\xi\xi\xi}(\xi) + \omega_f^2 W(\xi) - \omega_1^2 W(\xi) + \frac{1}{6} \omega_1^2 r^2 W_{,\xi\xi}(\xi) \\ - \omega_1^2 \left[ r_0 (1 - \xi) + \frac{1}{2} (1 - \xi^2) \right] W_{,\xi\xi}(\xi) + g \omega_f^\alpha W_{,\xi\xi\xi\xi}(\xi) \\ + \omega_1^2 (r_0 + \xi) W_{,\xi}(\xi) - \frac{1}{6} \omega_f^2 r^2 W_{,\xi\xi}(\xi) = 0, \end{aligned} \quad (20)$$

where  $\omega_f$  is a dimensionless complex frequency.

Substituting the dimensionless quantity into equations (17a) and (17d), respectively, the dimensionless boundary conditions of the fractional derivative viscoelastic beam can be expressed as follows:

$$W(0) = 0, \quad (21a)$$

$$W_{,\xi}(0) = 0, \quad (21b)$$

$$W_{,\xi\xi}(1) + g \omega_f^\alpha W_{,\xi\xi}(1) = 0, \quad (21c)$$

$$\begin{aligned} W_{,\xi\xi\xi}(1) - \frac{1}{6} r^2 \omega_f^2 W_{,\xi}(1) \\ + \frac{1}{6} r^2 \omega_1^2 W_{,\xi}(1) + g \omega_f^\alpha W_{,\xi\xi\xi}(1) = 0. \end{aligned} \quad (21d)$$

**3.4. Differential Quadrature Method.** When the differential quadrature method is used to solve the equation, most of the calculation accuracy will be determined by the selection of the weight function. Therefore, when using this method for calculation, the node distribution must be selected reasonably. For the equations of the specific problem to be solved, the properties of the solution region are different, often using nonuniform node partitioning, and more mesh points can be selected for regions close to the boundary where the physical properties change more prominently. And for the boundary region, the small variable  $\delta$  is used for the adjacency processing.

The values of the nodes by nonuniform sampling method are as follows:

$$\begin{aligned} \xi_1 &= 0, \\ \xi_2 &= \delta, \\ \xi_i &= \frac{1}{2} \left( 1 - \cos \frac{i-2}{N-3} \pi \right), \quad i = 3, 4, \dots, N-2, \\ \xi_{N-1} &= 1 - \delta, \\ \xi_N &= 1, \end{aligned} \quad (22)$$

where set  $\delta = 1 \times 10^{-6}$  and  $N = 13$  in subsequent calculation.

Then the discretization of equation (20) can be written as follows:

$$\begin{aligned}
& \sum_{j=1}^N A_{ij}^{(4)} W_j + \frac{1}{6} \omega_1^2 r^2 \sum_{j=1}^N A_{ij}^{(2)} W_j + g \omega_f^\alpha \sum_{j=1}^N A_{ij}^{(4)} W_j \\
& - \omega_1^2 \left[ r_0 (1 - \xi_i) + \frac{1}{2} (1 - \xi_i^2) \right] \sum_{j=1}^N A_{ij}^{(2)} W_j - \omega_1^2 W_i + \omega_f^2 W_i \\
& + \omega_1^2 (r_0 + \xi_i) \sum_{j=1}^N A_{ij}^{(1)} W_j - \frac{1}{6} \omega_f^2 r^2 \sum_{j=1}^N A_{ij}^{(2)} W_j = 0,
\end{aligned} \tag{23}$$

where  $A_{ij}^{(1)}$ ,  $A_{ij}^{(2)}$ ,  $A_{ij}^{(3)}$ , and  $A_{ij}^{(4)}$  are first-order, second-order, third-order, and fourth-order weight coefficients, respectively,

$$A_{ij}^{(1)} = \begin{cases} \frac{\prod_{k=1}^N (x_i - x_k)}{\prod_{k=1, k \neq i}^N (x_j - x_k)}, & i, j = 1, 2, \dots, N; i \neq j, \\ k \neq j \\ \sum_{k=1}^N \frac{1}{x_i - x_k}, & i, j = 1, 2, \dots, N; i = j, \\ k \neq i \end{cases}$$

$$A_{ij}^{(2)} = \sum_{k=1}^N A_{ik}^{(1)} A_{kj}^{(1)},$$

$$A_{ij}^{(3)} = \sum_{k=1}^N A_{ik}^{(1)} A_{kj}^{(2)}, \quad i, j = 1, 2, \dots, N,$$

$$A_{ij}^{(4)} = \sum_{k=1}^N A_{ik}^{(2)} A_{kj}^{(2)}. \tag{24}$$

The discretization of the boundary conditions is

$$W_1 = 0, \tag{25a}$$

$$\sum_{j=1}^N A_{2j}^{(1)} W_j = 0, \tag{25b}$$

$$(1 + g \omega_f^\alpha) \sum_{j=1}^N A_{N-1,j}^{(2)} W_j = 0, \tag{25c}$$

$$\begin{aligned}
& \sum_{j=1}^N A_{Nj}^{(3)} W_j - \frac{1}{6} r^2 \omega_f^2 \sum_{j=1}^N A_{Nj}^{(1)} W_j \\
& + \frac{1}{6} r^2 \omega_1^2 \sum_{j=1}^N A_{Nj}^{(1)} W_j + g \omega_f^\alpha \sum_{j=1}^N A_{Nj}^{(3)} W_j = 0.
\end{aligned} \tag{25d}$$

Equations (23), (25a) and (25d) can be written in matrix form:

$$(\omega_f^2 \mathbf{M} + \omega_f^\alpha \mathbf{C} + \mathbf{K}) \mathbf{W} = 0, \tag{26}$$

where  $\mathbf{M}$ ,  $\mathbf{C}$ , and  $\mathbf{K}$  are all  $(N-1)$  square matrix and  $\mathbf{W} = [W_2 \ W_3 \ \dots \ W_{N-1} \ W_N]^T$  is column matrix.

Thus, the generalized characteristic equation corresponding to equation (26) can be obtained as follows:

$$|\omega_f^2 \mathbf{M} + \omega_f^\alpha \mathbf{C} + \mathbf{K}| = 0, \tag{27}$$

where  $\mathbf{M}$ ,  $\mathbf{C}$  and  $\mathbf{K}$  contain the hub radius-beam length ratio, the slenderness ratio, the viscoelastic ratio, the dimensionless hub speed, fractional order, and dimensionless complex frequency of the system.

## 4. Numerical Results and Analyses

**4.1. Comparison and Verification.** The correctness and feasibility of the differential quadrature method used in this paper are analyzed by comparing the numerical results with reference [7]. In the case when  $g = 0$ ,  $\alpha = 0$ ,  $r = 0$ , and  $r_0 = 0.125$ , set the dimensionless hub speed at 0, 5, and 10, the result of the compared first three-order natural frequency with reference [7] is shown in Table 1:

It can be seen from the Table 1 that when the dimensionless hub rotational speed  $\omega_1$  is 0, 5, and 10 respectively, the dimensionless natural frequency of the system is basically the same as that of reference [7], and all errors are below 2%.

**4.2. Numerical Calculation and Analysis.** Considering the influence of moment of inertia, the effects of slenderness ratio  $r$ , the hub radius-beam length ratio  $r_0$ , viscoelastic ratio  $g$ , dimensionless hub speed  $\omega_1$ , and fractional order  $\alpha$  on the first three-order dimensionless  $\text{Im}(\omega_f)$  (imaginary part of complex frequency) and  $\text{Re}(\omega_f)$  (real part of complex frequency) of the fractional derivative rotating viscoelastic beam are analyzed.

Figure 3 plots the curves of complex frequency of the system with the hub radius-beam length ratio at  $r = 1/30$ ,  $g = 0.025$ ,  $\omega_1 = 10$ , and  $\alpha = 1/2$ . And we can see that the complex frequency of the system vary linearly with  $r_0$ , and  $r_0$  is positively correlated with the  $\text{Im}(\omega_f)$ , but negatively correlated with the  $\text{Re}(\omega_f)$ . With the increase of the order, the effect of  $r_0$  on the  $\text{Re}(\omega_f)$  is more obvious.

Figure 4 plots the curves of complex frequency of the system with slenderness ratio at  $r_0 = 0.25$ ,  $g = 0.025$ ,  $\omega_1 = 10$ , and  $\alpha = 1/2$ .

And we can see that when the slenderness ratio is between 0 and 0.08, slenderness ratio has less influence on the complex frequency of the system, and when slenderness ratio is between 0.08 and 0.10, the  $\text{Im}(\omega_f)$  of the system is negatively correlated with slenderness ratio, and the  $\text{Re}(\omega_f)$  increases first and then decreases. With the increase of the order of the system, the peak value of the  $\text{Re}(\omega_f)$  moves forward.

Figure 5 plots the curves of complex frequency of the system with viscoelastic ratio at  $r_0 = 0.25$ ,  $r = 1/30$ ,  $\omega_1 = 10$ , and  $\alpha = 1/2$ .

TABLE 1: Comparison of the first three dimensionless natural frequencies of elastic cantilever rotating beams at  $g = 0$ ,  $\alpha = 0$ ,  $r = 0$ , and  $r_0 = 0.125$ .

$\omega_1$	0		5		10	
	Present	Reference [7]	Present	Reference [7]	Present	Reference [7]
1st	3.515	3.507	6.302	6.425	10.953	11.159
2nd	22.029	21.647	24.951	24.973	32.122	32.965
3rd	60.673	59.207	65.011	63.539	73.672	71.497

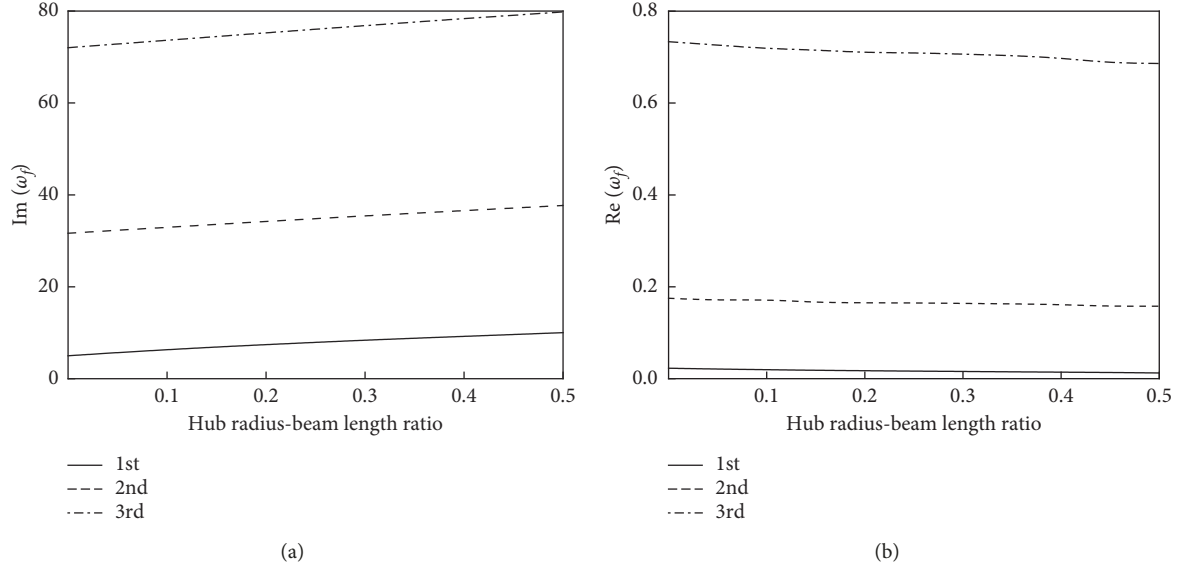


FIGURE 3: Variation curves of complex frequency of the system with the hub radius-beam length ratio at  $r = 1/30$ ,  $g = 0.025$ ,  $\omega_1 = 10$ , and  $\alpha = 1/2$ .

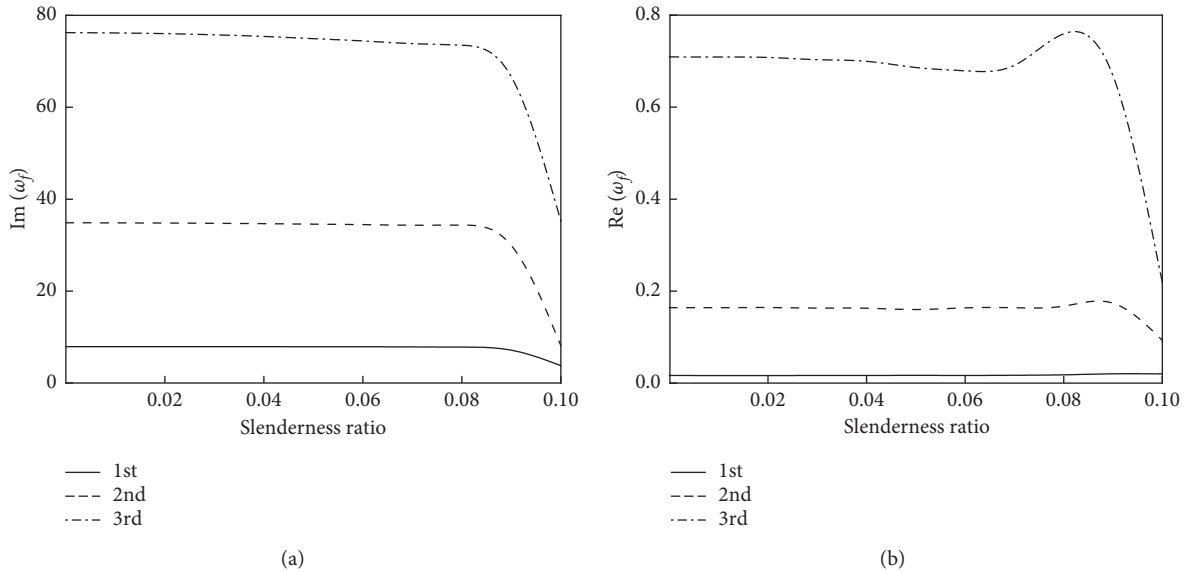


FIGURE 4: Variation curves of complex frequency of the system with slenderness ratio at  $r_0 = 0.25$ ,  $g = 0.025$ ,  $\omega_1 = 10$ , and  $\alpha = 1/2$ .

And we can see that the viscoelastic ratio has slight effect on the  $\text{Im}(\omega_f)$  of the system, and with the increase of the viscoelastic ratio, the  $\text{Im}(\omega_f)$  hardly changes. Meanwhile, the viscoelastic ratio has a great influence on the  $\text{Re}(\omega_f)$ , and

there is a positive correlation between them, and with the increase of order, the  $\text{Re}(\omega_f)$  increases more obviously. Therefore, the viscoelastic ratio can be used to describe the damping characteristics of materials.

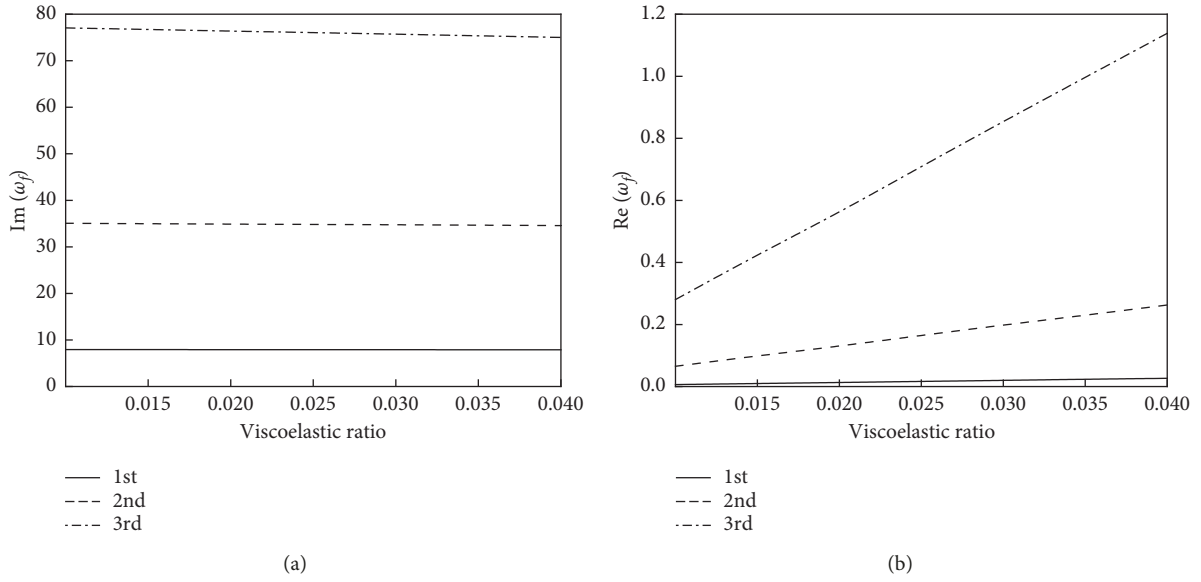


FIGURE 5: Variation curves of complex frequency of the system with viscoelastic ratio at  $r_0 = 0.25$ ,  $r = 1/30$ ,  $\omega_1 = 10$ , and  $\alpha = 1/2$ .

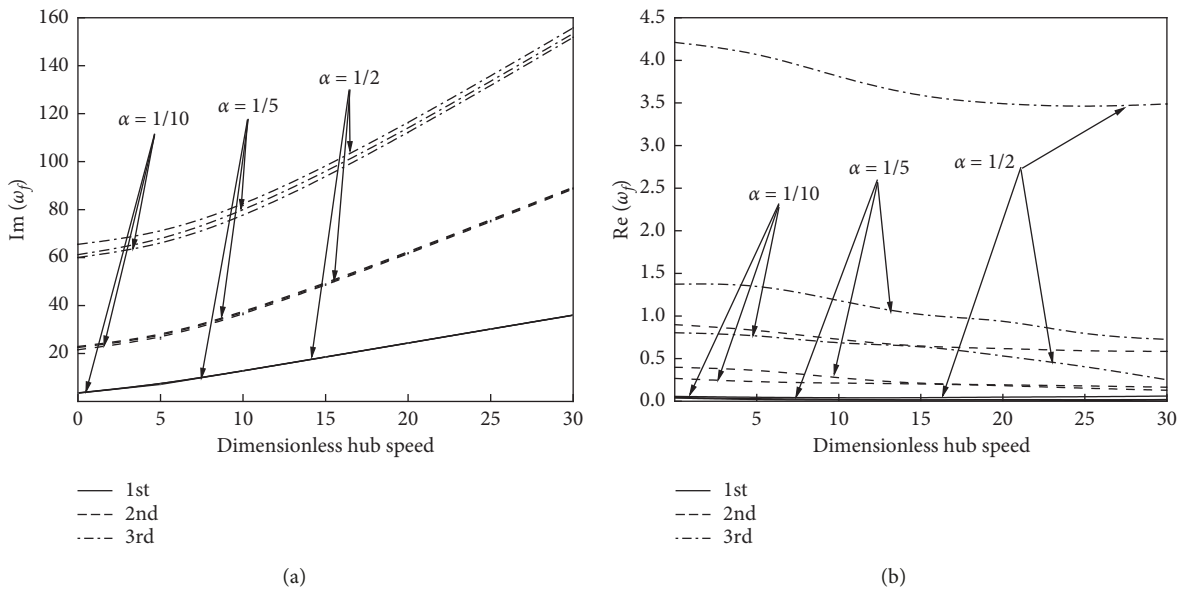


FIGURE 6: Variation curves of complex frequency of the systems at dimensionless hub speed with different fractional order at  $r_0 = 0.25$ ,  $r = 1/30$ , and  $g = 0.025$ .

Figure 6 plots the curve of complex frequency of the system with dimensionless hub speed at different fractional order  $\alpha = 1/10$ ,  $\alpha = 1/5$ , and  $\alpha = 1/2$  at  $r_0 = 0.25$ ,  $r = 1/30$ , and  $g = 0.025$ . And we can see that the dimensionless hub speed has a significant influence on the complex frequency of the system, and as the speed of the dimensionless hub increases, the  $\text{Im}(\omega_f)$  increases, the  $\text{Re}(\omega_f)$  decreases, and the attenuation of higher-order  $\text{Re}(\omega_f)$  becomes more obvious.

Meanwhile, fractional order has little effect on the  $\text{Im}(\omega_f)$  of the system, but the influence on the  $\text{Re}(\omega_f)$  is great, and the influence of fractional order on the high-order  $\text{Re}(\omega_f)$  is obvious. When  $\alpha = 1/2$ , the attenuation rate of the

$\text{Re}(\omega_f)$  is faster than  $\alpha = 1/5$ . Thus, viscoelastic materials with larger fractional order will be more conducive to the stability of the system.

**4.3. Response of Viscoelastic Rotating Beams with Kelvin–Voigt Fractional Derivatives.** For the system, set the number of mesh points  $N = 13$ , small variables  $\delta = 1 \times 10^{-6}$ , and nonuniform meshing of Kelvin–Voigt viscoelastic material beam with fractional derivative, when  $\xi_3 = 0.02447$ ,  $\xi_7 = 0.5$ ,  $\xi_{11} = 0.97553$ , and  $\xi_{13} = 1$ , and the response curve of different points on the viscoelastic beam is as follows Figure 7:

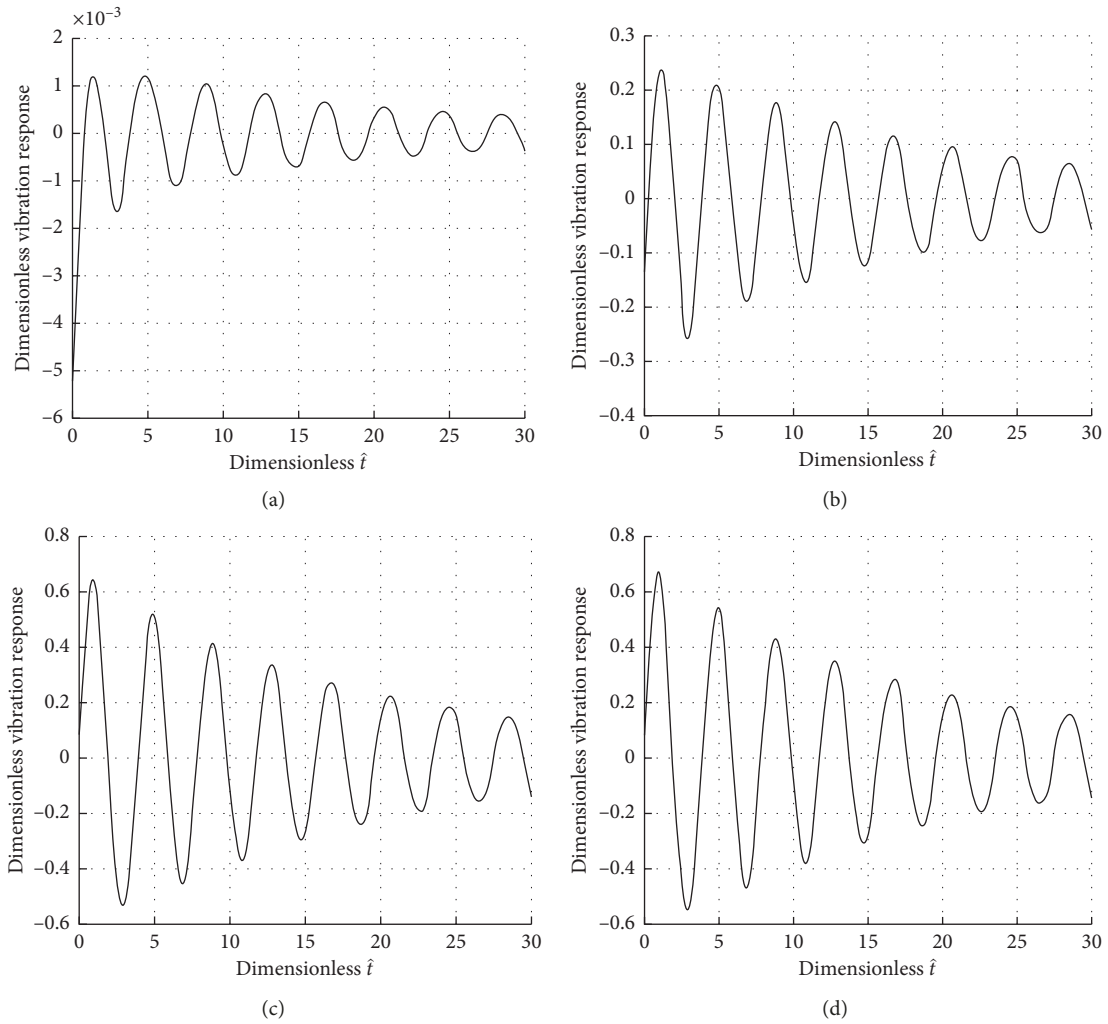


FIGURE 7: Vibration response curve of fractional derivative Kelvin–Voigt viscoelastic beam at  $r = 1/30$ ,  $r_0 = 0.25$ ,  $g = 0.025$ ,  $\omega_1 = 10$ , and  $\alpha = 1/2$ . (a)  $\xi_3 = 0.02447$ , (b)  $\xi_7 = 0.5$ , (c)  $\xi_{11} = 0.97553$ , and (d)  $\xi_{13} = 1$ .

Figure 7 plots the curves of response of the Kelvin–Voigt viscoelastic beam with fractional derivative when  $r_0 = 0.25$ ,  $r = 1/20$ ,  $g = 0.025$ ,  $\omega_1 = 10$ , and  $\alpha = 1/2$ . And we can see that the response at different points of the Kelvin–Voigt viscoelastic material beam.

As  $\xi_i$  increases, the corresponding response amplitude also increases, which indicates that the closer to the free end, the greater the response amplitude. Moreover, the amplitude of the system's response decreases with time, which is due to the damping effect in the material.

## 5. Conclusion

Based on Hamilton principle and Euler–Bernoulli beam theory, the influence of slenderness ratio, the hub radius–beam length ratio, dimensionless hub speed, viscoelastic ratio, and fractional order on the vibration characteristics of viscoelastic rotating beams with fractional derivatives is investigated by the differential quadrature method. The calculation results in this paper have little error with the existing literature, which shows the feasibility and correctness

of the differential quadrature method. Compared with other methods, the solving process of the differential quadrature method is more intuitive and easier to program.

When the dimensionless hub speed is constant, the dimensionless  $\text{Im}(\omega_f)$  and  $\text{Re}(\omega_f)$  of the system both increases slightly with the hub radius–beam length ratio increase. For a fractional derivative viscoelastic rotating hollow beam at a constant velocity, when slenderness ratio is about 0.08, the  $\text{Im}(\omega_f)$  and  $\text{Re}(\omega_f)$  have a sudden change; the former has been attenuating, while the latter has increased first and then decreased rapidly. The viscoelastic ratio has little effect on the  $\text{Im}(\omega_f)$  of the system, but it has a great influence on the  $\text{Re}(\omega_f)$ , and at high order, the  $\text{Re}(\omega_f)$  increases rapidly.

With the increase of dimensionless hub speed, the  $\text{Im}(\omega_f)$  of the system decreases, while the  $\text{Re}(\omega_f)$  increases, and the attenuation of higher-order  $\text{Re}(\omega_f)$  is more significant. Fractional order has little effect on the  $\text{Im}(\omega_f)$  of the system, but it has great influence on the  $\text{Re}(\omega_f)$ , and the effect on the higher-order  $\text{Re}(\omega_f)$  is more obvious.

Through the study of response at different points on a fractional derivative Kelvin–Voigt viscoelastic beam, we can

see that the response at different points on a viscoelastic beam varies with time in a wave function, and the closer to the fixed end, the smaller the amplitude of response. When near the free end, the amplitude of response is larger but the amplitude of the system's response decreases with time.

### Data Availability

The data used to support the findings of this study are available from the corresponding author upon request.

### Conflicts of Interest

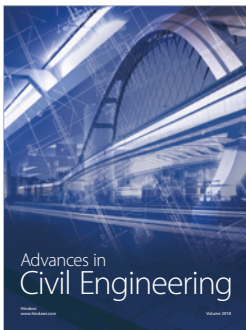
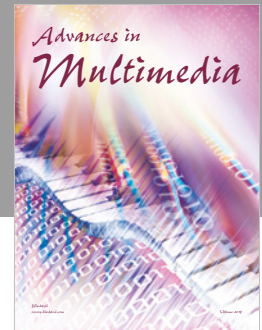
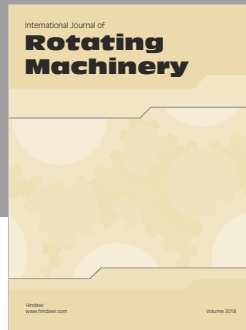
The authors declare that there are no conflicts of interest regarding the publication of this paper.

### Acknowledgments

Thanks are due to the support of the National Natural Science Foundation of China (Grant no. 11972286).

### References

- [1] J. R. Banerjee and H. Su, "Dynamic stiffness formulation and free vibration analysis of a spinning composite beam," *Computers & Structures*, vol. 84, no. 19-20, pp. 1208–1214, 2006.
- [2] J. Tian, J. Su, K. Zhou, and H. Hua, "A modified variational method for nonlinear vibration analysis of rotating beams including Coriolis effects," *Journal of Sound and Vibration*, vol. 426, no. 15, pp. 258–277, 2018.
- [3] T. Aksencer and M. Aydogdu, "Flapwise vibration of rotating composite beams," *Composite Structures*, vol. 134, no. 16, pp. 672–679, 2015.
- [4] Y. F. Zhang, E. C. Yang, and Y. H. Li, "Studies on nonlinear parametric vibration a rotating viscoelastic beam with variable cross-sections," *Journal of Dynamics and Control*, vol. 16, no. 5, pp. 418–423, 2018.
- [5] R. R. Li, Z. M. Wang, and X. S. Yao, "Vibration characteristics of rotating flexible ring beam made of functionally graded material," *Chinese Journal of Applied Mechanics*, vol. 34, no. 3, pp. 418–422, 2017.
- [6] B. K. Srivatsa and G. Ranjan, "Non-rotating beams isospectral to rotating Rayleigh beams," *International Journal of Mechanical Sciences*, vol. 142-143, no. 7, pp. 440–455, 2018.
- [7] A.-Y. Tang, X.-F. Li, J.-X. Wu, and K. Y. Lee, "Flapwise bending vibration of rotating tapered Rayleigh cantilever beams," *Journal of Constructional Steel Research*, vol. 112, no. 9, pp. 1–9, 2015.
- [8] A. H. Sofiyev and D. Hui, "On the vibration and stability of FGM cylindrical shells under external pressures with mixed boundary conditions by using FOSDT," *Thin-Walled Structures*, vol. 134, no. 1, pp. 419–427, 2019.
- [9] M. Yao, Y. Niu, and Y. Hao, "Nonlinear dynamic responses of rotating pretwisted cylindrical shells," *Nonlinear Dynamics*, vol. 95, no. 1, pp. 151–174, 2019.
- [10] J. R. Banerjee and D. R. Jackson, "Free vibration of a rotating tapered Rayleigh beam: a dynamic stiffness method of solution," *Computers & Structures*, vol. 124, no. 10, pp. 11–20, 2013.
- [11] S. Chakraverty and L. Behera, "Buckling analysis of nano-beams with exponentially varying stiffness by differential quadrature method," *Chinese Physics B*, vol. 26, no. 7, Article ID 074602, 2017.
- [12] H. B. Gao, L. Fu, and J. N. Niu, "Mechanical properties research on fractional derivative standard linear solid viscoelastic material," *Journal of Henan University (Natural Science)*, vol. 48, no. 1, pp. 86–91, 2018.
- [13] V. E. Tarasov, "No nonlocality: no fractional derivative," *Communications in Nonlinear Science and Numerical Simulation*, vol. 62, no. 9, pp. 157–163, 2018.
- [14] Z. Achouri, N. E. Amroun, and A. Benaissa, "The Euler-Bernoulli beam equation with boundary dissipation of fractional derivative type," *Mathematical Methods in the Applied Sciences*, vol. 40, no. 11, pp. 3837–3854, 2016.
- [15] R. Ansari, M. Faraji Oskouie, and R. Gholami, "Size-dependent geometrically nonlinear free vibration analysis of fractional viscoelastic nanobeams based on the nonlocal elasticity theory," *Physica E: Low-Dimensional Systems and Nanostructures*, vol. 75, no. 1, pp. 266–271, 2016.
- [16] S. M. S. Bahraini, M. Eghtesad, M. Farid, and E. Ghavanloo, "Large deflection of viscoelastic beams using fractional derivative model," *Journal of Mechanical Science and Technology*, vol. 27, no. 4, pp. 1063–1070, 2013.
- [17] P. Li and W. Ying, "Differential quadrature method for vibration analysis of beams on viscoelastic foundations," *Journal of Shanghai Normal University*, vol. 44, no. 2, pp. 143–149, 2015.
- [18] Q. Zhang, Y. F. Du, and Q. K. Zhu, "Study on large deformation mechanical behavior of Euler-Bernoulli beam using DQM," *Engineering Mechanics*, vol. 31, no. S1, pp. 1–4, 2014.
- [19] Z. G. Cao, "Static analysis of reinforced concrete beam using the differential quadrature method," *Chinese Quarterly of Mechanics*, vol. 4, pp. 749–756, 2015.
- [20] M. S. Matbuly, O. Ragb, and M. Nassar, "Natural frequencies of a functionally graded cracked beam using the differential quadrature method," *Applied Mathematics and Computation*, vol. 215, no. 6, pp. 2307–2316, 2009.
- [21] J. J. Li, Y. J. Hu, and C. J. Cheng, "Differential quadrature method for nonlinear dynamical behavior of a viscoelastic Timoshenko beam," *Journal of Vibration and Shock*, vol. 29, no. 4, pp. 143–146, 2010.
- [22] Z. Wang and R. Li, "Transverse vibration of rotating tapered cantilever beam with hollow circular cross-section," *Shock and Vibration*, vol. 2018, Article ID 1056397, 14 pages, 2018.
- [23] Y. F. Zhou and Z. M. Wang, "Application of the differential quadrature method to free vibration of viscoelastic thin plate with linear thickness variation," *Meccanica*, vol. 49, no. 12, pp. 2817–2828, 2014.



**Hindawi**

Submit your manuscripts at  
[www.hindawi.com](http://www.hindawi.com)

